Super-Coster-Kronig decay of Kr 3*p* core-hole states studied by multielectron coincidence spectroscopy

Y. Hikosaka,[1] P. Lablanquie,[2] T. Kaneyasu,[3] J. Adachi,[4] H. Tanaka,[4] I. H. Suzuki,[4,5] M. Ishikawa,[5] and T. Odagiri[5]

[1]*Institute of Liberal Arts and Sciences, University of Toyama, Toyama 930-0194, Japan*

[2]*Laboratoire de Chimie Physique Matière et Rayonnement (LCPMR), Sorbonne Université and CNRS, F-75005 Paris, France*

[3]*SAGA Light Source, Tosu 841-0005, Japan*

[4]*Photon Factory, Institute of Materials Structure Science, Tsukuba 305-0801, Japan*

[5]*Department of Materials and Life Sciences, Sophia University, Tokyo 102-8554, Japan*

(Received 4 March 2021; accepted 9 April 2021; published 27 April 2021)

Super Coster-Kronig (SCK) decay following Kr 3*p* photoionization has been investigated using a multielectron coincidence method. It is found that the SCK pathway occupies 23% of the $3p_{1/2}$ decay and only 2.5% of the $3p_{3/2}$ decay. The significant difference between the two 3*p* spin-orbit levels mainly results from the difference in energetics: almost all SCK transitions are energetically allowed in the $3p_{1/2}$ decay but only SCK transitions to the ^3F levels of $3d^{-2}$ are possible in the $3p_{3/2}$ decay. Subsequent decay processes from the SCK-final $3d^{-2}$ states are investigated, where a maximum of fivefold electron coincidences are analyzed.

DOI: 10.1103/PhysRevA.103.043119

I. INTRODUCTION

Decay by emitting an Auger electron is the predominant relaxation pathway of atomic inner-shell vacancies in the soft x-ray regime. The probabilities and energies of individual Auger transitions provide stringent tests for theoretical frameworks capturing electronic correlation and relativistic effects. Auger transitions of the Coster-Kronig (CK) type, in which an initial inner-shell vacancy is filled by an electron from a higher subshell in the same shell, exhibit remarkably large transition rates. One special case involving a large transition rate is the simultaneous ejection of electrons from the same shell; this is called a super Coster-Kronig (SCK) transition. When an SCK path is available for a core-hole state, its transition rate can be the dominant factor shortening the core-hole lifetime. However, theoretical estimation of SCK contributions in a core-hole decay is often very difficult, because the initial and final states of SCK processes tend to be very close in energy and the calculation accuracy of their state energies greatly affects the estimation of the magnitude of the SCK path.

The natural width of a 3*p* inner-shell vacancy generally shows an increasing trend with *Z*, but exhibits a peculiar reduction from Kr ($Z = 36$) to Rb ($Z = 37$) [1]. This can be ascribed to the closing of the $M_{2,3}M_{4,5}M_{4,5}$ SCK pathway in Rb [1,2]. For the adjacent Kr atom, the 3*p* natural width shows a marked difference between the spin-orbit levels (1.1 eV for $3p_{3/2}{}^{-1}$ and 1.3 eV for $3p_{1/2}{}^{-1}$ [3]). This suggests that SCK transitions are partly forbidden in Kr and different numbers of SCK transitions are allowed to 3*p* spin-orbit levels. The theoretical description of the SCK processes occurring between the closely lying levels is challenging, as pointed out in early theoretical studies [4,5]. A multiconfiguration Dirac-Fock calculation, calibrated using experimental state energies, suggested that all SCK transitions from the $3p_{3/2}{}^{-1}$ state are energetically forbidden and only about 34% of SCK transitions from the $3p_{1/2}{}^{-1}$ state are allowed [3]. In contrast, a large-scale configuration-interaction calculation indicated that all SCK transitions are energetically possible for both spin-orbit levels [6]. Experimental location of SCK transitions is highly desirable for understanding their contribution to the Kr 3*p* decay. Conventional Auger spectroscopy, however, hardly provides definite information about the SCK pathway, because slow electrons emitted by various other processes contribute to the low-kinetic energy portion of the Auger spectrum, preventing identification of the SCK structures.

The branching ratios of the ion charge states formed after Kr 3*p* ionization are expected to be strongly affected by the presence of SCK pathways. Photoelectron-photoion coincidence studies show that the fraction of Kr^{4+} is larger in the $3p_{1/2}$ decay than in the $3p_{3/2}$ decay [7,8]. The favorable Kr^{4+} formation in the $3p_{1/2}$ decay can stem from a larger contribution from SCK transitions, considering that the subsequent cascade decays from SCK-final $3d^{-2}$ states should end up largely in Kr^{4+} states. A threshold electron-ion coincidence study linked weak Kr^{5+} formation to 3*p* photoionization and proposed that the formation is associated with the subsequent decay of the SCK-final $3d^{-2}$ states [9]. The ion branching ratios from the 3*p* core-hole states were calculated using different approaches [3,10–12]. These calculations reproduced the experimental observations well, although it is hard to assess how each approach can properly determine the contributions from the SCK pathways.

In the present work, we employed multielectron coincidence spectroscopy, using a magnetic bottle electron spectrometer, to uncover the SCK pathways of Kr 3*p* core-hole states, where a maximum of fivefold electron coincidences were detected and analyzed. Thanks to the coincidence observation, the SCK transitions were isolated, and the relative

transition probabilities of the individual Auger decay pathways from the $3p^{-1}$ states were determined. Subsequent decay processes following the SCK transitions were also investigated.

II. EXPERIMENT

The experiment was carried out at the undulator beamline BL-2B at the Photon Factory. The 2.5-GeV electron storage ring was operated in hybrid-fill mode [13] under top-up injection. The bunch filling pattern comprises a train of low-current bunches (420 mA for 156 bunches) and a single high-current bunch (30 mA) located diametrically opposite the bunch train. Linearly polarized light from a planar undulator was monochromatized by a grazing incidence monochromator using a varied-line-spacing plane grating. A mechanical chopper [14], synchronized to the master clock of the storage ring operation, was used to select light pulses from the isolated single bunch. The achieved repetition rate of the light pulses was 229 kHz.

A magnetic-bottle-type electron spectrometer equipped with a 2.5-m flight tube was employed to perform multielectron coincidence spectroscopy. Electrons formed in the ionization region were captured over a 4π-*sr* solid angle by an inhomogeneous magnetic field and were guided towards the microchannel plate detector terminating the 2.5-m flight path. A small potential (−2.5 V) was applied to the permanent magnet, allowing zero energy electrons to reach the detector before the incidence of the next light pulse. Conversion from electron time-of-flight to kinetic energy was calibrated by measuring Ar $2p$ photoelectron lines at different photon energies and Kr $3d$ Auger lines. From the linewidths, the energy-resolving power of the spectrometer was estimated to be more than $E/\Delta E = 70$ above a kinetic energy of 30 eV. Below a kinetic energy of 30 eV, the energy-resolving power gradually drops with decreasing kinetic energy: $E/\Delta E$ is 40 at 10 eV and 20 at 5 eV.

A multielectron coincidence measurement was made for Kr at a photon energy of 355.2 eV (bandwidth of ∼20 meV). The photon energy, which is sufficiently higher than the $3p$ ionization thresholds (214.4 eV for $3p_{3/2}{}^{-1}$ and 222.2 eV for $3p_{1/2}{}^{-1}$ [15]), was chosen so that the photoelectrons do not much overlap in energy with the Auger electrons emitted in the decay of the $3p$ core holes. The accumulation time was about 8 h, with a count rate of around 4 kHz. While ∼12% of total electron counts were found to be produced by a leak of the bunch-train light, these electrons were effectively filtered out in the data analysis. This was possible because their flight times with respect to the isolated single bunch correspond to kinetic energies outside the expected energy range.

The electron detection efficiency of the spectrometer was determined by measuring the coincidences between Ar $2p$ photoelectrons and the associated Auger electrons at many different photon energies. The estimated values are plotted in Fig. 1, which can be well fitted by a double exponential decay function. The electron detection efficiency generally decreases with increasing kinetic energy, where the change is relatively rapid up to a kinetic energy of 100 eV and then tapers off. The intensities in all the spectra derived from the coincidence dataset and presented in this paper were corrected for the electron detection efficiency dependent on the electron energy. For example, the number of observed threefold coincidences was corrected by the inverse of the product of the detection efficiencies for the three electrons. Thus, the spectral intensities present the real number of events that occurred during the 8-h accumulation.

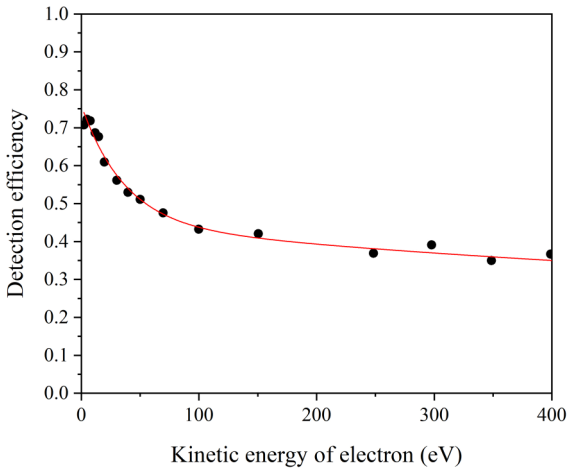

FIG. 1. Electron detection efficiency estimated from yields of coincidence between Ar $2p$ photoelectrons and the associated Auger electrons. Experimental values (black circles) were fitted with a double exponential decay function (solid red curve). Intensities in Figs. 2, 3, and 5–7 were corrected for the detection electron efficiency (see text for details).

III. RESULTS AND DISCUSSION

A. Auger decay pathways of the $3p^{-1}$ states

Figure 2(a) shows an inner-shell photoelectron spectrum of Kr. The energy resolution (∼2 eV for 140-eV electrons) is sufficient to practically resolve the $3p$ spin-orbit components, though the fine structures identified in a high-resolution photoelectron spectrum [15] cannot be recognized. The two-dimensional map in Fig. 2(b) displays the energy correlation between the photoelectrons in the range of Fig. 2(a) and Auger electrons below a kinetic energy of 120 eV. Knots of enhancements, lying vertically at the photoelectron energies for the $3d^{-1}$ and $3p^{-1}$ states, are seen on the map. Similar but weaker structures are observed at the photoelectron energies for the $3d^{-1}4l^{-1}nl$ shake-up satellite states. These vertical structures are formed by the Auger transitions from the core-hole states. On the left-hand side of the satellite structures, at least three diagonal stripes are identified. They result from the coincidence between the two photoelectrons emitted on core-valence double photoionization into the $3d^{-1}4l^{-1}$ states. While the present coincidence data include rich information about these individual processes, this article focuses only on the decay from the $3p^{-1}$ states. As for the Auger decay pathways from the $3d^{-1}$ states, the full details investigated by multielectron coincidence spectroscopy have already been reported [16,17].

The coincidence Auger spectra associated with the individual spin-orbit components of $3p^{-1}$ are shown in Fig. 3(a). These spectra essentially correspond to the vertical cuts of

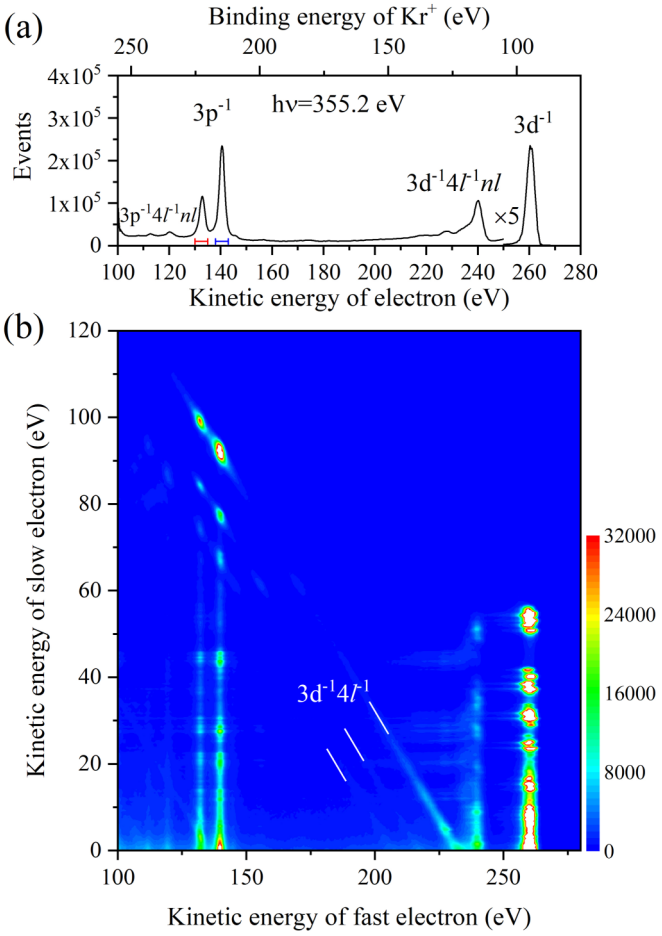

FIG. 2. (a) Inner-shell photoelectron spectrum of Kr at a photon energy of 355.2 eV, plotted in 0.2-eV steps. The two kinetic energy ranges for the extractions of coincidence events relevant to the $3p_{3/2}$ and $3p_{1/2}$ decays are indicated. (b) Two-dimensional map showing energy correlation between photoelectrons in the same range as in (a) and Auger electrons in the kinetic energy range of 0–120 eV. Color represents number of coincidences found in a box with dimensions of 0.4 eV (vertical) × 0.6 eV (horizontal).

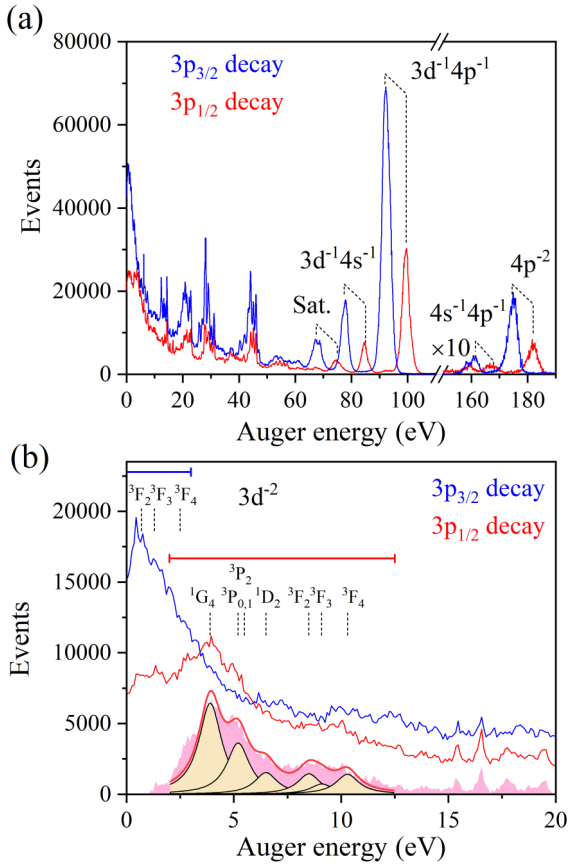

FIG. 3. Coincidence Auger spectra associated with the individual spin-orbit components of $3p^{-1}$: (a) whole range and (b) low kinetic energy portion. They are plotted with 0.1-eV steps. In the derivation of the spectra in (b), only the coincidence events including two additional electrons in the 0–60-eV kinetic energy range are used, in order to concentrate the contribution from the SCK transitions. In the extractions of the spectra in Figs. 5–7, the electrons in the energy ranges indicated in (b) were assumed to be SCK electrons. The pink-shaded curve, which is obtained by subtracting half the intensity of the $3p_{3/2}$ Auger spectrum from the $3p_{1/2}$ Auger spectrum, delineates the net SCK contribution in the $3p_{1/2}$ Auger spectrum. A fitting with the sum of seven Lorentzian peaks, whose widths and locations are fixed at the $3p_{1/2}$ natural width and at the estimated locations of the $3d^{-2}$ levels, respectively, is shown.

the two-dimensional map in Fig. 2(b) at the 3p photoelectron energies, but are obtained beyond the Auger energy range of the two-dimensional map, in order to view Auger structures of higher kinetic energy. For better statistics, these spectra were obtained by integrating the coincidence counts over the photoelectron ranges indicated in Fig. 2(a). The total intensity of the spectrum associated with the $3p_{3/2}$ decay is roughly twice as intense as that of the spectrum associated with the $3p_{1/2}$ decay, reflecting the statistical weight of the 3p spin-orbit levels.

The 3p Auger structures above a kinetic energy of 60 eV, which do not overlap with the 3d Auger transitions [see Fig. 2(b)], have already been studied by conventional Auger spectroscopy [3,18–20]. The two coincidence Auger spectra in Fig. 3(a) show similar peak profiles in that kinetic energy range, but the structures have shifted by as much as the 8-eV energy gap between the initial $3p_{1/2}{}^{-1}$ and $3p_{3/2}{}^{-1}$ levels. These structures result from first-step Auger decays of the 3p core-hole states. The weak structures seen in the kinetic energy range of 150–190 eV in Fig. 3(a) are associated with the $M_{2,3}N_{1,2,3}N_{1,2,3}$ Auger transitions forming Kr^{2+} final states with two valence holes. The three band structures exhibited in the kinetic energy range of 60–110 eV are produced by the $M_{2,3}M_{4,5}N_{1,2,3}$ CK transitions. The relative intensities of these Auger and CK transitions show no marked difference between the two core-hole states and agree fairly well with an observation based on conventional Auger spectroscopy [3] and calculations [3,6,10]. The wide natural widths of the initial 3p core-hole states prevent the individual Auger transitions constituting these band structures to be fully resolved even with a higher kinetic energy resolution. Jauhiainen *et al.* located the individual transitions by peak fitting to the band structures observed in a conventional Auger spectrum [3]. It should be noted that a spectral resolution beyond the limitation imposed by the natural widths of the core-hole states can be obtained

by making coincidences between the $4p$ photoelectron and the Auger electron, as was done for Ar $2s$ decay [21] or Xe $4d$ decay [22]. While such a resolution cannot be reached for the Kr $3p$ Auger lines with the present spectrometer resolution, it can be achieved by introducing electric retardation into the measurement [23].

In the coincidence Auger spectra of Fig. 3(a), the structures lying below a kinetic energy of 65 eV do not exhibit shifts according to the different initial $3p$ levels. Most peaks are associated with secondary Auger processes after the CK transitions. These structures are difficult to identify by conventional Auger spectroscopy because of severe overlap with the intense Auger lines associated with $3d$ photoionization. Below a kinetic energy of 20 eV, where the appearance of SCK structures is anticipated, both coincidence spectra show a gradual increase with decreasing kinetic energy. These distributions result partly from triple Auger decay constituted by an initial CK transition and subsequent emissions of two additional Auger electrons [24]. Besides, false coincidences with electrons emitted from the apparatus surface may contribute to these distributions. These contributions to the low kinetic energy region prevent us from tangibly locating the SCK transitions.

The SCK transitions lead to the formation of Kr^{2+} states with double $3d$ holes. A calculation [6] indicates that the subsequent decay predominantly emits two additional Auger electrons, according to the sequential filling of the $3d$ holes (i.e., $3d^{-2} \rightarrow 3d^{-1}4l^{-2} \rightarrow 4l^{-4}$). Such sequential filling of two core holes is the normal decay path of double core-hole states [25]. Owing to the subsequent decay, the electron emitted in the SCK transition can be observed in coincidence with a $3p$ photoelectron and two additional Auger electrons. The two additional Auger electrons have kinetic energies of less than 60 eV (see Fig. 4). The electron spectra derived from such coincidence events are plotted in Fig. 3(b), where a $3p_{3/2}$ or $3p_{1/2}$ photoelectron is selected. Figure 3(b) shows that the coincidence filter effectively removes the secondary Auger electrons relevant to the CK pathway, appearing above a kinetic energy of 10 eV in Fig. 3(a). In addition, the intensities of the background distributions are reduced in Fig. 3(b), because of the removal of the contribution from triple Auger decay initiated by the CK transition. It should be noted that the weak peaks remaining in 15–20 eV are due to the transitions ($3d^{-1}4p^{-2} \rightarrow 4s^{-1}4p^{-3}$) following the SCK transitions, proving that the coincidence filter works reasonably well.

The $3p_{1/2}$ Auger spectrum in Fig. 3(b) exhibits, at around a kinetic energy of 4 eV, an apparent enhancement lying on the background distribution gradually increasing with decreasing kinetic energy. This enhancement is ascribable to the SCK transition from the $3p_{1/2}{}^{-1}$ state. No corresponding structure can be identified at the same kinetic energy in the $3p_{3/2}$ Auger spectrum, which is reasonable, given the first-step Auger decay from the $3p$ spin-orbit levels. The shaded curve presented in Fig. 3(b) delineates the net enhancement in the $3p_{1/2}$ spectrum, which was obtained by subtracting half the intensity of the $3p_{3/2}$ Auger spectrum from the $3p_{1/2}$ Auger spectrum. The subtraction is justified if the contribution from the SCK transitions is negligible in the $3p_{3/2}$ Auger spectrum. In practice, considering the SCK contribution in the $3p_{3/2}$ Auger spectrum, oversubtraction is anticipated in the range

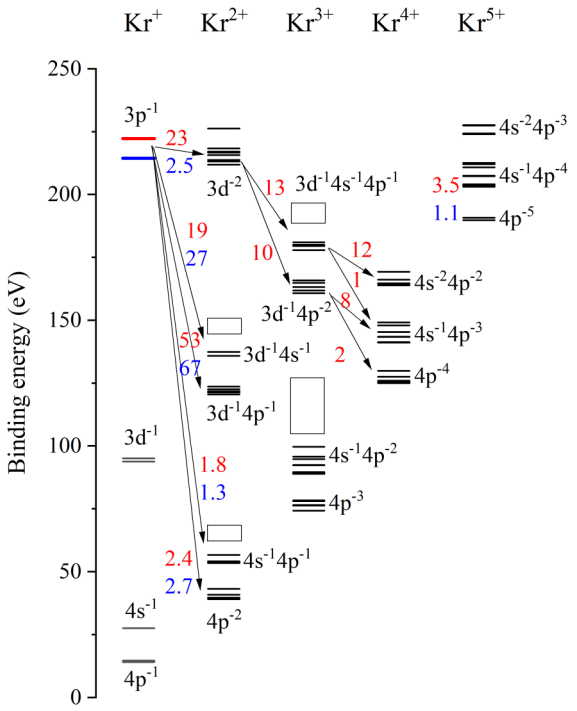

FIG. 4. Energy levels of Kr ion states lying below 240 eV, where energetically crowded levels are simplified. The numbers indicate the branching ratios (in %) of the decay pathways from the $3p^{-1}$ states, where the values for the $3p_{1/2}$ and $3p_{3/2}$ decays are written in red and blue, respectively.

below 3 eV. Apart from the broad peak already observed at around a kinetic energy of 4 eV, a broad structure extending up to 12 eV is identified in the shaded curve.

The energy locations of the SCK transitions to Kr^{2+} $3d^{-2}$, estimated from the interpretation of the $L_{2,3}M_{4,5}M_{4,5}$ band in the Kr $2p$ Auger spectrum [26] and the binding energies of the $2p^{-1}$ and $3p^{-1}$ states [15,27], are indicated in Fig. 3(b). While the accumulation of the uncertainties in these experimental values could result in a sizable error in the estimated locations, the structures seen in the shaded curve correspond well to the estimated $3d^{-2}$ locations. In practice, the structures are reasonably reproduced by a fitting with the sum of seven Lorentzian peaks whose widths and locations are fixed at the $3p_{1/2}$ natural width and the estimated locations of the $3d^{-2}$ levels, respectively. This implies that the observed structures can be allocated to the SCK transitions and also that the $3d^{-2}$ locations are reasonably estimated from the literature values. The relative intensities of the SCK transitions to the $3d^{-2}$ levels, determined by the fitting, are $^1G_4 : {}^3P_{0,1} : {}^3P_2 : {}^1D_2 : {}^3F_2 : {}^3F_3 : {}^3F_4 = 1 : 0.56(10) : 0.0(1) : 0.24(4) : 0.22(5) : 0.11(5) : 0.22(3)$. They show a certain resemblance to those formed by the $L_2M_{4,5}M_{4,5}$ transition in Kr, though the formation of the $^1G_4$ level has a larger share in the $2p_{1/2}$ decay (66.3% in the total $L_2M_{4,5}M_{4,5}$ transition) [26].

It is clearly revealed here that almost all the SCK transitions (except for the $^1S_0$ level lying 7.1 eV above the $^1G_4$ level) are energetically allowed in the $3p_{1/2}$ decay. In contrast, only the SCK transitions to the ^3F levels of $3d^{-2}$ are energetically

possible in the $3p_{3/2}$ decay. The $3p_{3/2}$ Auger spectrum shows an enhancement around the locations of the ^3F levels, but the intensity is not much more than twice that of the $3p_{1/2}$ Auger spectrum in the same kinetic energy range. As shown in the next section, we find that the SCK transitions to the ^3F levels are weakly included in the $3p_{3/2}$ Auger spectrum, and the corresponding coincidence counts are only one-sixth of those of the total SCK transitions in the $3p_{1/2}$ decay. The fitting to the $3d^{-2}$ structures in the shaded curve indicates that the formation of the ^3F levels shares one-third of the total SCK transitions from the $3p_{1/2}{}^{-1}$ state. Considering also that the initial population of the $3p_{3/2}{}^{-1}$ state is twice that of the $3p_{1/2}{}^{-1}$ state, the total SCK intensity in the $3p_{3/2}$ decay, observed as one-sixth of that in the $3p_{1/2}$ decay, is considerably weaker than expected. This observation may imply that the SCK transition rates become unfavorable for small transition energies.

The branching ratios of the first-step Auger transitions from the $3p$ core-hole states are presented in the energy diagram of Fig. 4. These values were estimated from the relative intensities of the corresponding structures in Figs. 3(a) and 3(b). The errors in the estimated branching ratios are mainly caused by the inaccuracy of the detection efficiency, and are anticipated to be smaller than 20% for each value. Apart from these decay paths, direct double Auger decay into Kr^{3+} levels, in which two Auger electrons are simultaneously ejected from the $3p$ core-hole filling, can also contribute to the $3p$ decay. However, closer inspection of the present coincidence data failed to reveal such a contribution. This is striking contrast to the detectable contributions from direct double Auger paths in the decays of Ne $1s$ [28], Ar $2p$ [29], Kr $3d$ [16], and Xe $4d$ [30]. The CK and SCK transitions have large transition rates in the Kr $3p$ case, and thus the direct double Auger paths become less favorable in the Kr $3p$ decay.

The most striking difference between the branching ratios of the $3p_{3/2}$ and $3p_{1/2}$ decays is that the contribution from the SCK pathway occupies 23% in the $3p_{1/2}$ decay but only 2.5% in the $3p_{3/2}$ decay. As clarified above, this difference basically results from the fact that almost all the SCK channels are energetically open for the $3p_{1/2}$ decay but only limited channels are allowed for the $3p_{3/2}$ decay. A large-scale configuration-interaction calculation suggested that basically all the SCK transitions are energetically possible for both the spin-orbit levels and the contributions share 23.5% of the $3p_{3/2}$ decay and 35.5% of the $3p_{1/2}$ one [6]. This calculation reasonably estimates the SCK contribution in the $3p_{1/2}$ decay, while inaccurate location of the energy level positions results in the apparent overestimation of the SCK contribution in the $3p_{3/2}$ decay. A multiconfiguration Dirac-Fock calculation suggested that the SCK transitions share over 58% of the total $3p$ decay [3]. The overestimation of the SCK contribution is due mainly to the inaccurate estimations of the positions of the relevant energy levels.

Assuming that the rates for the decay paths other than the SCK transition are the same for the $3p_{3/2}$ and $3p_{1/2}$ decays, the total decay rate of the $3p_{1/2}{}^{-1}$ state becomes approximately 20% larger than that of the $3p_{3/2}{}^{-1}$ state, due to the extra contribution from the SCK transitions in the $3p_{1/2}$ decay. This estimation is consistent with the 20% larger natural width of the $3p_{1/2}{}^{-1}$ state relative to that of the $3p_{3/2}{}^{-1}$ one [3].

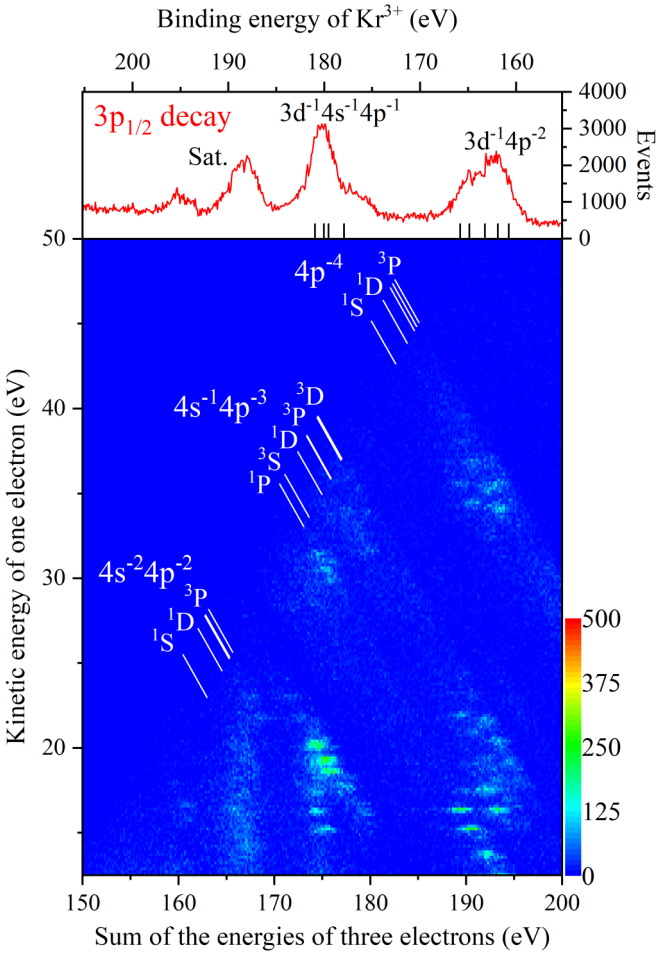

FIG. 5. Two-dimensional map showing subsequent decay of $3d^{-2}$ states populated by SCK transitions from $3p_{1/2}{}^{-1}$. Correlations between $Kr^{3+}3d^{-1}4l^{-2}$ states formed from $3d^{-2}$ and the energy of slow Auger electrons emitted in further decay are shown. The map was derived from fourfold coincidences including a $3p_{1/2}$ photoelectron and an electron in the SCK electron range (2–12.5 eV) indicated in Fig. 3(b). Colors represent number of coincidences found in a box with dimensions 0.17 eV (vertical) × 0.17 eV (horizontal). The top panel shows the spectrum of the energy sum of $3p$ photoelectron, SCK electron, and faster Auger electron. This spectrum delineates structures of Kr^{3+} $3d^{-1}4l^{-2}$ states formed from $3d^{-2}$, when the faster Auger electron is emitted in the initial Auger decay from $3d^{-2}$ states. The step size is 0.1 eV.

B. Subsequent decay processes after the super-Coster-Kronig transitions

In this section, we investigate the subsequent decays from the $3d^{-2}$ states formed by the SCK transitions. The $3d^{-2}$ states should decay predominantly by the sequential fillings of the double $3d$ holes. The two Auger electrons emitted in the decays from the $3d^{-2}$ states can be detected as a fourfold coincidence together with a $3p$ photoelectron and an SCK electron. The top panels in Figs. 5 and 6 show the spectra of the energy sum of three electrons ($3p$ photoelectron, SCK electron, and faster Auger electron), derived from fourfold coincidences including a $3p_{1/2}$ and $3p_{3/2}$ photoelectron, respectively. Here, electrons in the

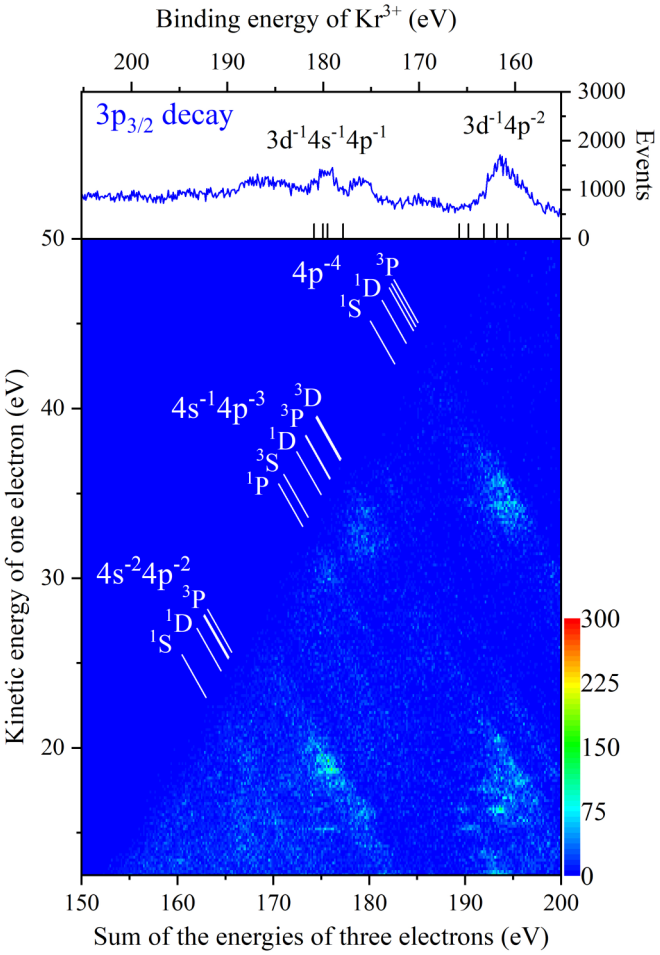

FIG. 6. Same as in Fig. 5, but for the $3p_{3/2}$ decay. The map was derived from fourfold coincidences including a $3p_{3/2}$ photoelectron and an electron in the SCK electron range (0–3 eV) indicated in Fig. 3(b).

energy ranges indicated in Fig. 3(b) were assumed to be SCK electrons. Supposing that the faster Auger electron is emitted in the initial Auger decay from the $3d^{-2}$ states, these spectra should delineate the structures of the Kr^{3+} $3d^{-1}4l^{-2}$ states formed after the initial Auger decay from $3d^{-2}$. The spectra are thus plotted as a function of the binding energy of Kr^{3+}, by using the relation (binding energy of Kr^{3+}) = (photon energy)–(energy sum of the three electrons).

Reflecting the sizable contribution from the SCK electron in the selected energy range for the $3p_{1/2}$ decay, clear band structures allocatable to $Kr^{3+}3d^{-1}4l^{-2}$ states appear in the $3p_{1/2}$ spectrum (top panel of Fig. 5). By referring to a configuration-interaction calculation [6], the band structure around binding energies of 165 and 180 eV can be assigned to $3d^{-1}4p^{-2}$ and $3d^{-1}4s^{-1}4p^{-1}$, respectively. The structures above a binding energy of 180 eV are ascribed to satellite states, and the calculation suggested a large contribution from the configuration of $3d^{-1}4p^{-3}nd$ to the satellite states [6]. The two-dimensional map in Fig. 5 reveals correlations between the Kr^{3+} states and the energies of the slow Auger electrons emitted in further decay. Island structures clearly observed on the map correspond to transitions from $Kr^{3+}3d^{-1}4l^{-2}$ to Kr^{4+} $4l^{-4}$. On this map, structures for the formation of a given Kr^{4+} state should lie on a diagonal line, $x + y =$ const, because the available energy shared among the four electrons emitted in Kr^{4+} formation is fixed.

While the individual Kr^{3+} levels in the $3d^{-1}4l^{-2}$ bands are hard to resolve in the top panel, the island structures associated with these Kr^{3+} levels are distinguishable on the map, thanks to the different energies of the subsequent Auger transitions. We can identify at least six different Kr^{3+} energy levels (binding energies of 160.5, 161.8, 163.0, 163.2, 164.5, and 165.7 eV) in the $3d^{-1}4p^{-2}$ band and at least four different Kr^{3+} energy levels (binding energies of 175.6, 179.9, 180.0, and 181.0 eV) in the $3d^{-1}4s^{-1}4p^{-1}$ band. The branching ratios of the first- and second-step Auger transitions from the $3d^{-2}$ states formed in the $3p_{1/2}$ decay, determined from the intensities of the structures in Fig. 5, are indicated in the energy diagram of Fig. 4. These values do not agree well with the calculation results [6].

The two-dimensional energy correlation map in Fig. 6 is similar to that in Fig. 5 but for the $3p_{3/2}$ decay. Island structures resembling those identified in the $3p_{1/2}$ decay are seen. A comparison between the total intensities of the island structures in Figs. 5 and 6 reveals that the intensity of the initial SCK transition in the $3p_{3/2}$ decay is about one-sixth of that in the $3p_{1/2}$ decay. This value allows us to estimate the branching ratio of the SCK transition in the $3p_{3/2}$ decay.

Since the $3p^{-1}$ spin-orbit levels lie energetically above the Kr^{5+} threshold (see Fig. 4), they can proceed by quadruple Auger decay and contribute to the formation of Kr^{5+} ions. In practice, the weak formation of Kr^{5+} associated with the $3p$ decay was observed by photoelectron-photoion coincidence spectroscopy [8,9]. Figure 7(a) plots histograms of the energy sums of five electrons detected as fivefold coincidence including a $3p$ photoelectron. The spectra for the $3p_{1/2}$ and $3p_{3/2}$ decays exhibit peaks for the formations of the Kr^{5+} $4p^{-5}$ and $4s^{-1}4p^{-4}$ levels. The formation of these Kr^{5+} levels is barely visible in a histogram obtained by excluding the $3p$ photoelectron (not shown). This implies that the observed Kr^{5+} formation is essentially due to the quadruple Auger decay from $3p^{-1}$ and contributions from other processes (for instance, direct double-core photoionization to $4d^{-2}$ and the subsequent decay) are negligible in Fig. 7(a). Since the available energy shared by the four electrons emitted in the $3p$ decay is at most 33 eV, at least one of the electrons always has a kinetic energy assumed as a SCK electron. Accordingly, it is difficult to isolate the contribution from the pathway via an intermediate formation of $3d^{-2}$.

Matsui *et al.* attributed their observation of Kr^{5+} in coincidence with the $3p$ threshold photoelectron to the process $3p^{-1} \rightarrow 3d^{-2} \rightarrow 3d^{-1}4p^{-3} \rightarrow 4p^{-5}$ [9]. In this process, two electrons are simultaneously emitted in the first decay step from intermediate $3d^{-2}$ states. On the other hand, a configuration interaction calculation [6] predicts that the Kr^{5+} formation results from the fully stepwise decay $3p^{-1} \rightarrow 3d^{-2} \rightarrow 3d^{-1}4p^{-3}5d \rightarrow 4s^{-1}4p^{-4}5d \rightarrow 4p^{-5}$. The energy distributions of electrons for the formation of the Kr^{5+} $4p^{-5}$ levels are shown in Fig. 7(b). Structures corresponding to SCK transitions that result in intermediate $3d^{-2}$ formations are visible in both curves, suggesting important

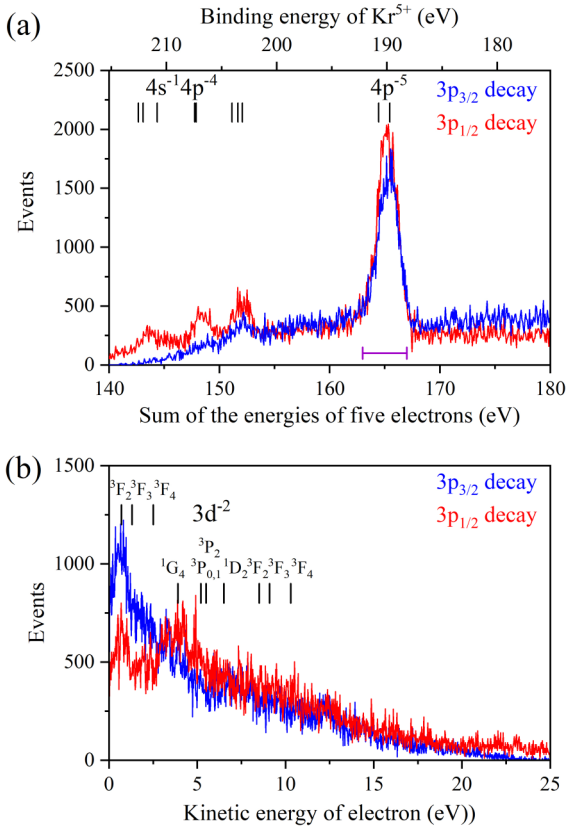

FIG. 7. (a) Histograms of the kinetic energy sum of the five electrons including a $3p_{1/2}$ or $3p_{3/2}$ photoelectron, which is plotted in steps of 0.07 eV. (b) Energy distributions of electrons ejected upon the formation of Kr^{5+} $4p^{-5}$ levels. The range of the kinetic energy sum, selected to derive these distributions, is indicated in (a). The step size is 0.025 eV.

contributions from the intermediate $3d^{-2}$ formation, however, the poor statistics prevent us from being able to identify such structures as revealing the pathway to the final Kr^{5+} formation.

The number of events associated with the Kr^{5+} formation in Fig. 7(a) compared to the number of $3p$ photoelectrons in Fig. 2(a) gives the probability of a $3p$ hole to end as Kr^{5+}. We estimate it to be 3.5% and 1.1% in the total decays from the $3p_{1/2}{}^{-1}$ and $3p_{3/2}{}^{-1}$ states, respectively. The estimated Kr^{5+} branching ratios are roughly consistent with the observations made by photoelectron-photoion coincidence spectroscopy (less than $2 \pm 2\%$ for both $3p^{-1}$ states [8]). On the other hand, a threshold electron-ion coincidence study estimates the branching ratios to be 7% and 4% for the $3p_{1/2}{}^{-1}$ and $3p_{3/2}{}^{-1}$ states, respectively [9]. Apart from the disagreement in the absolute values, the more favorable formation in the $3p_{1/2}$ decay agrees with the present observation. Considering the branching ratios of the $3d^{-2}$ formation (23% in the $3p_{1/2}$ decay and 2.5% in the $3p_{3/2}$ decay), the Kr^{5+} branching ratio in the $3p_{3/2}$ decay is quite favorable. This suggests that Kr^{5+} formation does not result solely from the decay of the $3d^{-2}$ states. Other paths that may possibly be contributing to Kr^{5+} formation include double Auger decay of the $3p^{-1}$ states into $3d^{-1}4p^{-3}5d$ and the subsequent decay.

IV. CONCLUSIONS

The SCK decay from Kr $3p$ core-hole states and the subsequent decay processes are investigated by multielectron coincidence spectroscopy. It is found that the contribution from the SCK pathway occupies 23% of the $3p_{1/2}$ decay and only 2.5% of the $3p_{3/2}$ decay. The difference stems from the fact that almost all SCK transitions are energetically allowed in the $3p_{1/2}$ decay while only the SCK transitions to the ^3F levels of $3d^{-2}$ are energetically possible in the $3p_{3/2}$ decay. The $3d^{-2}$ states formed by SCK transitions decay predominantly through sequential fillings of the double $3d$ holes, which is identified in fourfold coincidences. Moreover, the formation of Kr^{5+} states in the $3p$ decay is observed as fivefold coincidences.

ACKNOWLEDGMENTS

The authors are grateful to the Photon Factory staff for stable operation of the PF ring. This work was performed with the approval of the Photon Factory Program Advisory Committee (Proposals No. 2018G619 and No. 2018S2-003).

[1] M. Ohno and G. A. van Riessen, J. Electron Spectrosc. Relat. Phenom. **128**, 1 (2003).
[2] H. Aksela, S. Aksela, and R. Lakanen, Phys. Rev. A **42**, 1791 (1990).
[3] J. Jauhiainen, A. Kivimäki, S. Aksela, O.-P. Sairanen, and H. Aksela, J. Phys. B: At. Mol. Opt. Phys. **28**, 4091 (1995).
[4] S. Svensson, N. Mårtensson, E. Basilier, P. Å. Malmquist, U. Gelius, and K. Siegbahn, Phys. Scr. **14**, 141 (1976).
[5] M. Ohno and G. Wendin, J. Phys. B: At. Mol. Phys. **11**, 1557 (1978).
[6] V. Jonauskas, S. Kučas, and R. Karazija, Phys. Rev. A **84**, 053415 (2011).
[7] S. Brünken, Ch. Gerth, B. Kanngießer, T. Luhmann, M. Richter, and P. Zimmermann, Phys. Rev. A **65**, 042708 (2002).
[8] Y. Tamenori, K. Okada, S. Tanimoto, T. Ibuki, S. Nagaoka, A. Fujii, Y. Haga, and I. H. Suzuki, J. Phys. B: At. Mol. Opt. Phys. **37**, 117 (2004).
[9] T. Matsui, H. Yoshii, A. Higurashi, E. Murakami, T. Aoto, T. Onuma, Y. Morioka, A. Yagishita, and T. Hayaishi, J. Phys. B: At. Mol. Opt. Phys. **35**, 3069 (2002).
[10] A. G. Kochur, V. L. Sukhorukov, A. I. Dudenko, and P. V. Demekhin, J. Phys. B: At. Mol. Opt. Phys. **28**, 387 (1995).
[11] A. H. Abdullah, A. M. El-Shemi, and A. A. Ghoneim, Radiat. Phys. Chem. **68**, 697 (2003).
[12] V. Jonauskas, R. Karazija, and S. Kučas, J. Phys. B: At. Mol. Opt. Phys. **41**, 215005 (2008).
[13] R. Takai, T. Obina, Y. Tanimonot, T. Honda, M. Shimada, Y. Kobayashi, and T. Mitsuhashi, Proc. IPAC **10**, 2564 (2010).

[14] J. Adachi, H. Tanaka, T. Kosuge, H. Ishii, I. H. Suzuki, T. Kaneyasu, T. Taniguchi, T. Odagiri, S. Ohtaki, Y. Tsuji, K. Soejima, P. Lablanquie, and Y. Hikosaka, J. Phys.: Conf. Ser. **1412**, 152092 (2020).

[15] S. Svensson, B. Eriksson, N. Mårtensson, G. Wendin, and U. Gelius, J. Electron Spectroec. Relat. Phenom. **47**, 327 (1988).

[16] J. Palaudoux, P. Lablanquie, L. Andric, K. Ito, E. Shigemasa, J. H. D. Eland, V. Jonauskas, S. Kučas, R. Karazija, and F. Penent, Phys. Rev. A **82**, 043419 (2010).

[17] E. Andersson, S. Fritzsche, P. Linusson, L. Hedin, J. H. D. Eland, J.-E. Rubensson, L. Karlsson, and R. Feifel, Phys. Rev. A **82**, 043418 (2010).

[18] W. Mehlhorn, Z. Phys. **187**, 21 (1965).

[19] A. Hiltunen, H. Aksela, S. Aksela, S. Ricz, and Gy. Víkor, J. Phys. B **33**, 2881 (2000).

[20] J. J. Jureta, B. P. Marinković, and L. Avaldi, J. Quant. Spectrosc. Radiat. Transfer **268**, 107638 (2021).

[21] P. Lablanquie, F. Penent, R. I. Hall, H. Kjeldsen, J. H. D. Eland, A. Muehleisen, P. Pelicon, Ž. Šmit, M. Žitnik, and F. Koike, Phys. Rev. Lett. **84**, 47 (2000).

[22] J. Viefhaus, G. Snell, R. Hentges, M. Wiedenhöft, F. Heiser, O. Geßner, and U. Becker, Phys. Rev. Lett. **80**, 1618 (1998).

[23] Y. Hikosaka, M. Sawa, K. Soejima, and E. Shigemasa, J. Electron Spectrosc. Relat. Phenom. **192**, 69 (2014).

[24] Hikosaka *et al.* (unpublished).

[25] P. Lablanquie, F. Penent, and Y. Hikosaka, J. Phys. B: At. Mol. Opt. Phys. **49**, 182002 (2016).

[26] J. C. Levin, S. L. Sorensen, B. Crasemann, M. H. Chen, and G. S. Brown, Phys. Rev. A **33**, 968 (1986).

[27] F. Wuilleumier, J. Phys. (Paris) **32**, C4-88 (1971).

[28] Y. Hikosaka, T. Kaneyasu, P. Lablanquie, F. Penent, E. Shigemasa, and K. Ito, Phys. Rev. A **92**, 033413 (2015).

[29] P. Lablanquie, L. Andric, J. Palaudoux, U. Becker, M. Braune, J. Viefhaus, J. H. D. Eland, and F. Penent, J. Electron. Spectroec. Relat. Phenom. **156–158**, 51 (2007).

[30] F. Penent, J. Palaudoux, P. Lablanquie, L. Andric, R. Feifel, and J. H. D. Eland, Phys. Rev. Lett. **95**, 083002 (2005).